Assessment of Scattering of Plane Waves on Optically Illuminated Area of Rough Surface

Hanaa H. Qamer[1, *], Asmaa E. Farahat[2],
Khalid F. A. Hussein[2], and Mohamed B. El-mashade[1]

Abstract—In this paper, a new robust computational method that applies the geometrical theory of diffraction (GTD) in conjunction with the ray tracing (RT) technique is developed to evaluate the electromagnetic scattering pattern due to a plane wave incident on a rough surface of quite arbitrary statistical parameters. The Fresnel reflection model is applied under the assumption of arbitrary electrical and optical properties of the rough surface material to obtain the scattering patterns for both the power reflected to the upper half-space and the power transmitted into the medium covered by the rough surface. Also the polarization of the plane wave primarily incident on the rough surface is taken into consideration. The algorithm developed in the present work accounts for multiple bounces of an incident ray and, hence, it can be considered arbitrary higher-order GTD-RT technique. The accuracy of the obtained results is verified through the comparison with the experimental measurements of the scattering pattern of a light beam incident on rough sheets with specific statistical properties. Also, some of the obtained results are compared to other published results using the geometrical optics (GO) and the second-order Kirchhoff's approximation. The numerical results of the present work are concerned with investigating the dependence of the scattering pattern on the surface roughness, refractive index, angle of incidence, and the resolution of the geometric model of the rough surface. Also, it is shown that for limited resolution of the rough surface model, the accuracy of the calculated scattered field depends on the angle of incidence of the primary beam and the surface roughness.

1. INTRODUCTION

Studying electromagnetic (EM) scattering from random rough surfaces, especially in the visible and infrared spectral range, is of great importance for many applications and scientific research purposes. The characterization of rough surfaces through the investigation of the EM and light scattering finds wide fields of scientific research [1–8]. One of the most important applications is the optical tomography, in which the scattering patterns for a beam incident on an objective material provide extensive information such as the surface roughness and optical properties. The characterization of the materials and devices used in VLSI manufacturing is usually accomplished by studying the light scattered from the surfaces of such constituents. Both theoretical and experimental investigation of EM scattering from rough surfaces has great importance in many scientific, commercial, and military applications such as the earth remote sensing for studying the ocean surface and the terrain at long length scales [9–11]. Inner wall coating inside a building can be considered as random rough surfaces, which have significant effects on the indoor Optical Wireless Communication (OWC) especially those implementing diffuse topology. The study of optical scattering from rough surfaces is necessary for the design and performance assessment of such OWC systems [12]. An ideal "matte" or diffusely reflecting surface has Lambertian reflectance

property which is greatly recommended for OWC that implement diffuse topology. In other words, the Lambertian surface's luminance is isotropic, and the luminous intensity obeys Lambert's cosine law.

Some analytic and semi-analytic techniques have been proposed for evaluating the EM scattering from rough surfaces [13–31]. These include (i) the small-amplitude perturbation theory, in which the scattered field is expanded in powers of the surface profile function through linear terms, (ii) the Kirchhoff approximation, in which the scattering is treated as reflection from the plane tangent to the surface at each point, (iii) the extinction theorem in which the scattering equations, based on this theorem are solved numerically and, finally, (iv) the techniques based on the Rayleigh scattering equation. In [21], the relationship between the pattern of the scattered light and the statistical properties of the scattering surface given by Beckmann-Kirchhoff theory is utilized to measure the surface roughness through an iterative procedure proposed by inverting this relationship, to retrieve the height autocorrelation function. In [23], the scattering of electromagnetic waves from a rough surface is treated using the extinction theorem. The angular distribution of the ensemble average of reflected and transmitted field intensities are calculated. In this method, one-dimensional profiles for the rough surface are generated through a Monte Carlo method to solve the scattering equations numerically. In [24], a numerical solution of the reduced Rayleigh equation for the scattering of light from two-dimensional penetrable rough surfaces is achieved. The pattern of the light scattered from the surface is calculated by considering a horizontally or vertically polarized light wave incident on two-dimensional Gaussian or cylindrical rough surfaces of either isotropic or anisotropic statistical properties.

The second-order Kirchhoff approximation [31], also known as the iterated physical optics, consists of the first two terms of a Neumann expansion of the magnetic field integral equation. The modified second-order Kirchhoff approximation (KA) proposed in [30] can give the results that agree well with those obtained by the Monte Carlo numerical simulations and in experiments, using the angular and the propagation shadowing functions introduced in their solutions for accounting for the effects of the higher order scattering. The geometrical optics (GO) approximation model for assessment of electromagnetic scattering on rough surfaces can be obtained as the infinite frequency limit of the physical optics model. The GO approximation [28, 29] implements ray tracing to follow the electromagnetic energy incident on the rough surface with the possible subsequent multiple bounces on the points of the rough surface. This is done for each ray until it leaves the rough surface. It takes into consideration the shadowing made by the rough surface elements through ray tracing. Each point on which a ray falls is modeled as a locally optically smooth surface where Fresnel approximation is applicable.

A summary of other techniques used for the assessment of electromagnetic scattering from rough surfaces is provided in [16]. The methods reviewed in [16] include the Meecham-Lysanov method, phase-perturbation method, small-slope approximation, operator expansion method, tilt-invariant approximation, local weight approximation, weighted curvature approximation, Wiener-Hermite approach, unified perturbation expansion, full-wave approach, improved Green's function methods, volumetric method and integral equation method.

The present paper applies the Geometrical Theory of Diffraction (GTD) in conjunction with the Ray Tracing (RT) to account for scattering of optical waves and other electromagnetic waves from rough surfaces. Such GTD-RT technique accounts for higher order scattering by considering multiple bounces of the ray incident on a rough surface. Moreover, the Fresnel reflection and transmission coefficients are calculated to take into consideration the effect of the material of the rough surface. This method is applicable for random rough surfaces of both metallic and dielectric materials with quite arbitrary statistical parameters. The proposed GTD-RT technique is fully numerical and avoids the approximations encountered in the analytical or semi-analytical techniques that result in significant inaccuracies (except for the high frequency formulation which is the spirit of the ray theory).

The numerical results for the scattering pattern evaluated using the GTD-RT method is investigated through experimental verification. The polarization of the plane wave incident on the rough surface is taken into consideration. The present work investigates the dependence of the accuracy of the resulting scattering pattern on the resolution of the geometric model of the rough surface. Also, it studies the dependence of the accuracy of the calculated scattered field on the angle of incidence of the primary beam and the surface roughness.

2. GENERATION OF RANDOM ROUGH SURFACE MODEL

Rough surfaces with Gaussian height distribution and Gaussian correlation function are single-scale surfaces as they have band-limited spectrum. Owing to the well-known statistical characteristics of Gaussian surfaces, a great deal of research has been conducted to treat such type of rough surfaces. Gaussian rough surfaces are completely defined statistically by the correlation length, L_c and the root-mean-squared height, h_{rms}. In the present analysis, it is assumed that, for isotropic rough surface, the correlation function is power exponential or Gaussian and can be expressed as follows.

$$C\left(d\right) = h_{rms}^2 \exp\left(-\frac{d^2}{L_c^2}\right), \tag{1}$$

where d is the horizontal distance between two correlated points on the rough surface.

The slope of the surface can be calculated as the second moment of the power spectrum. A rough surface with Gaussian correlation function is known to have its surface slope expressed as: $s = \sqrt{2}h_{rms}/L_c$; the surface roughness in the present study is defined as follows.

$$R_D = \sqrt{2}s = \frac{2h_{rms}}{L_c} \tag{2}$$

Let the dimensions of the surface be $L_x \times L_y$ which is discretized to $Q_x \times Q_y$ points (vertices) along x and y directions, respectively. The correlation lengths are L_{cx} and L_{cy} along x and y directions, respectively. The coordinates of each point in surface are (x, y, z), where z is the random height whereas x and y represent a uniform horizontal grid. The horizontal distances between two adjacent points are Δx and Δy along x and y directions, respectively. The roughness degree of such a surface depends on the ratio between h_{rms} and the correlation length. For a square isotropic surface, $L_{cx} = L_{cy} = L_c$, $L_x = L_y = L$, $Q_x = Q_y = Q$, and $\Delta x = \Delta y = \Delta$. For such a surface, let N_{Lc} be the number of the surface points taken along the correlation length, and hence, L_c can be calculated as follows

$$L_c = (N_{Lc} - 1)\Delta \tag{3}$$

To generate a rough surface numerically, a two-dimensional array of discrete Gaussian random numbers with zero-mean, $\mu = 0$, and a standard deviation $\sigma = h_{rms}$ are generated. These random numbers represent the heights of the discrete points on the random surface. In this manner the heights are uncorrelated. To get a rough surface model with a specific correlation length, a Savitzky-Golay filter (SGF) with a correlation window size of N_{Lc} is applied to smooth the rows and then the columns of the generated array of random numbers [32]. The mean value of the resulting (smoothed) array is subtracted from the values of the array elements which are then scaled to get their standard deviation equal to the required root-mean-squared height of the surface. It is shown in [32] using a variogram measurement of the geometric model of the rough surface generated by the proposed method, that the required statistical parameters (L_c and h_{rms}) as well as the Gaussian correlation function are accurately satisfied in the resulting model of the rough surface.

3. EVALUATION OF OPTICAL WAVE SCATTERING ON RANDOM ROUGH SURFACES

This section is concerned with the evaluation of the optical scattering from random rough surfaces with arbitrary statistical parameters using the GTD in conjunction with the RT technique. The geometrical model of the rough surface is created as described in Section 2 such that the plane of incidence is parallel to xz plane as shown in Figure 1. The plane wave polarization is considered vertically polarized (V-polarized) if the electric field lies completely in the plane of incidence and is considered horizontally polarized (H-polarized) if the electric field lies completely in the plane parallel to the xy plane. The direction of incidence of the plane wave is defined by θ_i, which is the angle between the propagation vector $\mathbf{k}_i$ and the positive z-axis, whereas $\theta_i^{(n)}$ is the conventionally known angle of incidence, which is the supplementary of θ_i.
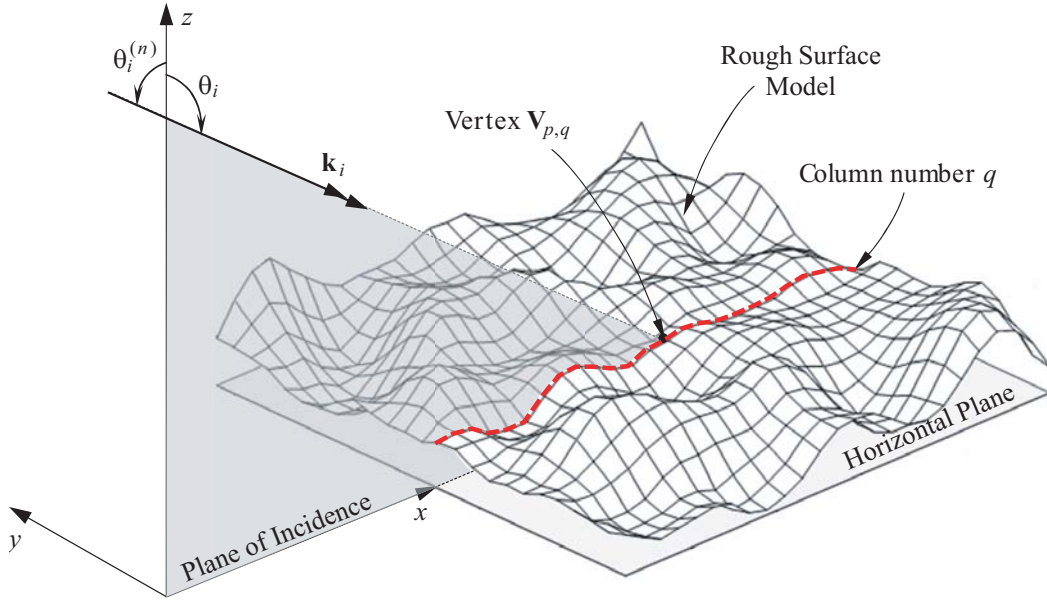
Figure 1. All the vertices on the qth column of the rough surface model are coplanar and lie in the plane of incidence: $y = (q - 1)\Delta y$.

3.1. Applicability of the GTD-RT Technique for Optical Scattering on Rough Surfaces

Logically, for the geometric optics approximation, on which the GTD relies, the wavelength should be very small relative to the dimensions of the details of the scattering surface such as the nuts, curvatures, and so on to get accurate assessment of electromagnetic scattering. Consequently, for a rough surface subjected to an incident electromagnetic wave, it is persuasive that the following conditions should be satisfied to get accurate results using the GTD-RT.

$$\lambda \ll L_c\sqrt{1+R_D^2} \tag{4a}$$

Persuasively, the last condition (4a) may be satisfied for $\lambda \sim 0.1 L_c\sqrt{1+R_D^2}$. However, it is shown by numerical experiments, in Section 4 of the present work, that accurate results can still be obtained using the GTD-RT for $\lambda \sim L_c\sqrt{1+R_D^2}$. It is shown in [28] that the GO approximation still gives accurate results for the scattering from rough surfaces (under some conditions) even for $\lambda \approx 0.65 L_c$.

To get accurate numerical assessment of the optical wave scattering on such a surface using the GTD-RT technique, the following condition should be satisfied

$$\lambda \gg \Delta \tag{4b}$$

If the conditions given by Eq. (4) are satisfied, the GTD-RT technique can be applied to evaluate the scattering of an optical beam incident on such rough surface model.

3.2. Application of GTD-RT for Assessment of Scattering of Parallel Rays on Rough Surfaces

This section provides a detailed description of the proposed GTD-RT technique when being applied to evaluate the optical and EM scattering due to a plane wave illuminating a rough surface as shown in Figure 1. The incident plane wave is represented by a number of rays; each ray is associated with an amount of power that is to be calculated so as to satisfy uniform power distribution over the transverse plane of the incident wave. The phase associated with each of the scattered rays is obtained by calculating the total distance travelled during ray tracing. The rough surface absorption or reflectance is evaluated by calculating the Fresnel coefficients at the point of incidence. Finally, a method is proposed

to calculate the scattering pattern over the upper half space and the the transmission pattern over the lower half space. Both first order and higher order ray tracing are described through systematic algorithm facilitated to be applied as a simulation tool for optical and EM scattering on rough surfaces.

The random rough surface is discretized to a grid of vertices arranged uniformly in the x and y directions and separated by steps Δx and Δy, respectively. The number of vertices along x and y directions are P and Q, respectively. Each vertex of this uniform grid has a random height $z_{p,q}$, where the indices p and q refer to the vertex row and column of the grid in the x and y directions respectively. Thus, the position vector of a vertex on the rough surface can be expressed as

$$\mathbf{V}_{p,q} = x_{p,q}\hat{a}_x + y_{p,q}\hat{a}_y + z_{p,q}\hat{a}_z \tag{5}$$

where,

$$x_{p,q} = p\Delta x, \quad y_{p,q} = q\Delta y \tag{6}$$

Each vertex of the gird representing the rough surface is connected with the adjacent vertices using triangular meshing. The normal vector at each vertex of the surface is the average of the normal vectors of the adjacent triangular patches sharing this vertex.

The procedure to apply the proposed GTD-RT method is detailed in the following subsections.

3.2.1. Ray Representation of the Incident Plane Wave

The vector propagation constant of the incident plane wave can be expressed as

$$\mathbf{k}_i = k_o\hat{a}_{k_i} = k_o\left(\hat{a}_x k_{i_x} + \hat{a}_z k_{i_z}\right) \tag{7}$$

where k_o is the free space wavenumber, $\hat{a}_{k_i}$ the unit vector in the direction of propagation, and

$$k_{i_x} = \sin\theta_i, \quad k_{i_z} = \cos\theta_i \tag{8}$$

The incident plane wave is represented by a number of parallel rays by setting a ray incident on each vertex $\mathbf{V}_{p,q}$ of the rough surface. Each ray is associated with an amount of power $\mathfrak{p}_{i_{p,q}}$ which is determined so as to satisfy uniform power density distribution over the transverse plane. Without any loss in generality, it is assumed that the propagation unit vector of the plane wave $\hat{a}_{k_i}$ is always in the xz plane (the squint angle is zero). Consider the transverse plane (normal to $\hat{a}_{k_i}$) that passes through the point $\mathbf{O}_q = (0, y_{p,q}, 0)$. The transverse plane intercepts the plane $y = y_{p,q}$ in the line $\mathscr{L}_{i_q}$ that passes through the point $\mathbf{O}_q$.

3.2.2. Calculating the Power Associating Each of the Incident Rays

Starting from the 1st row of vertices of the mesh representing the rough surface and moving sequentially to the Qth row, the following procedure is applied to scan the vertices on the qth row, $\mathbf{V}_{p,q}$, sequentially from $p = 1$ to $p = P$:

1- From each vertex $\mathbf{V}_{p,q}$, draw a line perpendicular to the transverse plane of the incident wave as shown in Figure 2, and find the intersection point υ_p whose position vector relative to the point $\mathbf{O}_q$ is $\upsilon_p = (\xi_{p,q}, 0, \zeta_{p,q})$. This can be achieved as follows.

$$\upsilon_p \cdot \hat{a}_{k_i} = 0 = \xi_{p,q} k_{i_x} + \zeta_{p,q} k_{i_z} \tag{9}$$

Let $\Delta_{i_{p,q}}$ be the distance from the intersection point υ_p to the vertex $\mathbf{V}_{p,q}$; consequently one has

$$\mathbf{V}_{p,q} = \upsilon_p + \Delta_{i_{p,q}}\hat{a}_{k_i} \tag{10}$$

This relation can be split into the following scalar equations

$$\xi_{p,q} = x_{p,q} - k_{i_x}\Delta_{i_{p,q}} \tag{11a}$$

$$\zeta_{p,q} = z_{p,q} - k_{i_z}\Delta_{i_{p,q}} \tag{11b}$$

Equations (9), (11a), and (11b) can be solved together to get $\Delta_{i_{p,q}}$, $\xi_{p,q}$ and $\zeta_{p,q}$ as follows. Substitute from Eqs. (11a), (11b) into Eq. (9) and make use of Eq. (8) to get

$$\Delta_{i_{p,q}} = x_{p,q}\sin\theta_i + z_{p,q}\cos\theta_i \tag{12}$$

Figure 2. The plane of incidence $y = (q-1)\Delta y$. Application of the ray tracing technique to calculate the scattering of plane waves on rough surfaces.

2- Define $\xi_{\max}$ as the maximum value of x-component of v_p evaluated during the progress of scanning the vertices on the qth row sequentially from $p = 1$ to $p = P$. Initially set $\xi_{\max} = 0$, and define a flag variable $\Upsilon_{p,q}$ for the incident ray at this vertex.

With scanning the vertices on the qth row moving from left to right, the index p increases by one for each vertex where the intersection point v_p is calculated as described above and the value of $\xi_{\max}$ is updated; that is, if $\xi_{p,q} > \xi_{\max}$, then this ray is considered active ($\Upsilon_{p,q} = 1$) and the $\xi_{\max}$ is updated as $\xi_{\max} = \xi_{p,q}$. If $\xi_{p,q} \leq \xi_{\max}$, then the ray incident on this vertex is considered inactive ($\Upsilon_{p,q} = 0$), which means that the vertex (p,q) is shadowed (blocked) from the incident wave by some part of the surface. Consequently, the ray $i_{p,q}$ does not contribute to the scattered field, which

implies that the power associating this ray should be set to zero. As shown in Figure 2, the area illuminated by each incident ray on the transverse plane are not equal and can be expressed as,

$$\Lambda_{p,q} = \frac{1}{2} \left(L_R + L_L \right) \Delta y \tag{13}$$

where L_R is the distance between the point υ_p and the nearest right-hand point, υ_{p_R}, on the line $\mathscr{L}_{i_q}$ corresponding to an active ray, and L_L is the distance between the point υ_p and the nearest left-hand point, υ_{p_L}, corresponding to an active ray. Thus, one has

$$L_R = |\upsilon_{p_R} - \upsilon_p| \tag{14a}$$
$$L_L = |\upsilon_{p_L} - \upsilon_p| \tag{14b}$$

Consequently, to get uniform power density on the transverse plane, the power associating each ray $\mathfrak{p}_{i_{p,q}}$ should be proportional to $\Lambda_{p,q}$ and, hence, can be expressed as,

$$\mathfrak{p}_{i_{p,q}} = \Lambda_{p,q} P_d \tag{15}$$

where P_d is the power density of the incident plane wave.

3.2.3. Calculating the Directions of the Reflected Rays

In the microscopic study of the scattering from a rough surface it is assumed that the surface of the region around the point (vertex) of incidence is locally smooth; thus, the Snell's law can be applied to get the unit vector in the direction of the reflected ray. The ray $\mathfrak{i}_{p,q}$ incident on the rough surface at the vertex $\mathbf{V}_{p,q}$, makes an angle ϑ_i with $\hat{a}_{n_{p,q}}$ which is the unit vector normal to surface at this vertex. The reflected ray at the same vertex is $\mathfrak{r}_{p,q}$; it lies in the same plane of $\hat{a}_{k_i}$ and $\hat{a}_{n_{p,q}}$ and makes an angle $\vartheta_r = \vartheta_i$ with $\hat{a}_{n_{p,q}}$ as shown in Figure 2. Hence, the unit vector $\hat{a}_{k_{r_{p,q}}}$ in the direction of the reflected ray $\mathfrak{r}_{p,q}$ can be determined as follows

$$\hat{a}_{k_{r_{p,q}}} = \hat{a}_{k_i} + 2 \cos \vartheta_i \hat{a}_{n_{p,q}} \tag{16}$$

The unit vector $\hat{a}_{k_{r_{p,q}}}$ can be written in terms of its components as follows

$$\hat{a}_{k_{r_{p,q}}} = k_{rx_{p,q}} \hat{a}_x + k_{ry_{p,q}} \hat{a}_y + k_{rz_{p,q}} \hat{a}_z \tag{17}$$

3.2.4. Calculating the Phases Associating the Reflected Rays

To calculate the phase associated with each reflected ray $\mathfrak{r}_{p,q}$, the path difference travelled by this ray, $\Delta_{r_{p,q}}$ shown in Figure 2, should be evaluated. From each vertex, $\mathbf{V}_{p,q}$, the normal to the wave front of the reflected ray is drawn as shown in Figure 2. It is required to find the intersection point ν_p whose position vector relative to the point $\mathbf{O}_q$ is $\nu_{p,q} = (\alpha_{p,q} \beta_{p,q} \gamma_{p,q})$. This can be achieved as follows.

$$\nu_{p,q} \cdot \hat{a}_{k_{r_{p,q}}} = 0 = \alpha_{p,q} k_{rx_{p,q}} + \beta_{p,q} k_{ry_{p,q}} + \gamma_{p,q} k_{rz_{p,q}} \tag{18}$$

Let $\Delta_{r_{p,q}}$ be the distance from the vertex $\mathbf{V}_{p,q}$ to the intersection point $\nu_{p,q}$. Thus,

$$\nu_{p,q} = \mathbf{V}_{p,q} - \Delta_{r_{p,q}} \hat{a}_{k_{r_{p,q}}} \tag{19}$$

This can be written in scalar equations as follows,

$$\alpha_{p,q} = x_{p,q} - k_{rx_{p,q}} \Delta_{r_{p,q}} \tag{20a}$$
$$\beta_{p,q} = y_{p,q} - k_{ry_{p,q}} \Delta_{r_{p,q}} \tag{20b}$$
$$\gamma_{p,q} = z_{p,q} - k_{rz_{p,q}} \Delta_{r_{p,q}} \tag{20c}$$

Equations (18), (20a), (20b), and (20c) can be solved together to get $\Delta_{r_{p,q}}$, as follows

$$\Delta_{r_{p,q}} = x_{p,q} k_{rx_{p,q}} + x_{p,q} k_{ry_{p,q}} + z_{p,q} k_{rz_{p,q}} \tag{21}$$

Thus, the phase associated with the $\mathfrak{r}_{p,q}$ can be expressed as,

$$\Delta \Phi_{rp,q} = \frac{2\pi}{\lambda} \left(\Delta_{i_{p,q}} - \Delta_{r_{p,q}} \right) \tag{22}$$

3.2.5. Calculating the Directions of the Transmitted Rays

The Snell's law can be applied at the vertex of incidence to get the unit vector in the direction of the transmitted ray. The transmitted ray at the vertex $\mathbf{V}_{p,q}$ is $\mathfrak{t}_{p,q}$; it lies in the same plane of $\hat{a}_{k_i}$ and $\hat{a}_{n_{p,q}}$ and makes an angle ϑ_t with the vector $-\hat{a}_{n_{p,q}}$. The relation between ϑ_i and ϑ_t is given by,

$$n_1 \sin \vartheta_i = n_2 \sin \vartheta_t \tag{23}$$

Hence, the unit vector $\hat{a}_{k_{t_{p,q}}}$ in the direction of the transmitted ray $\mathfrak{t}_{p,q}$ can be determined as follows

$$\hat{a}_{k_{t_{p,q}}} = \frac{n_1}{n_2} \hat{a}_{k_i} + \left(\frac{n_1}{n_2} \cos \vartheta_i - \cos \vartheta_t \right) \hat{a}_{n_{p,q}} \tag{24}$$

The unit vector $\hat{a}_{k_{t_{p,q}}}$ can be written in terms of its components as follows

$$\hat{a}_{k_{t_{p,q}}} = k_{tx_{p,q}} \hat{a}_x + k_{ty_{p,q}} \hat{a}_y + k_{tz_{p,q}} \hat{a}_z \tag{25}$$

3.2.6. Calculating the Phases Associating the Transmitted Rays

To calculate the phase associated with each transmitted ray $\mathfrak{t}_{p,q}$, the path difference travelled by this ray, $\Delta_{t_{p,q}}$ as shown in Figure 2, should be evaluated. In a way similar to that followed to calculate the path difference $\Delta_{r_{p,q}}$, of the reflected ray, one can arrive at the following expression for $\Delta_{t_{p,q}}$.

$$\Delta_{t_{p,q}} = x_{p,q} k_{tx_{p,q}} + x_{p,q} k_{ty_{p,q}} + z_{p,q} k_{tz_{p,q}} \tag{26}$$

Thus, the phase associated with the $\mathfrak{t}_{p,q}$ can be expressed as,

$$\Delta \Phi_{tp,q} = \frac{2\pi}{\lambda} \left(\Delta_{i_{p,q}} - \Delta_{t_{p,q}} \right) \tag{27}$$

3.2.7. Calculating the Fresnel Coefficients at the Points of Reflection

The ray, $\mathfrak{i}_{p,q}$, suffers reflection and transmission at the point of incidence, $\mathbf{V}_{p,q}$, as shown in Figure 3. The directions of the reflected and transmitted rays are determined according to the direction of the normal to the surface at this point and the angles ϑ_i, ϑ_r, ϑ_t shown in Figure 3. The Snell's law of optical reflection is applied to determine these angles.
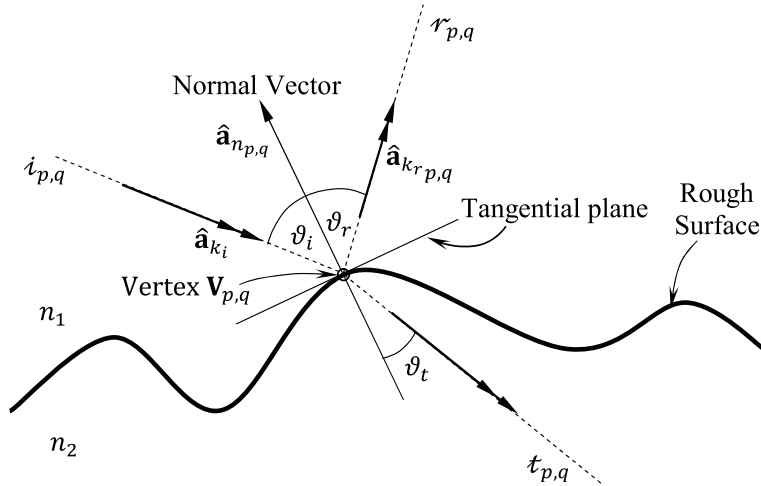
Figure 3. Fresnel reflection at a vertex on the rough surface.

The power $\mathfrak{p}_{r_{p,q}}$ associating the ray $\mathfrak{r}_{p,q}$ reflected at the vertex $\mathbf{V}_{p,q}$ can be related to the power associating the ray $\mathfrak{i}_{p,q}$ incident at the same vertex through the following relation.

$$\mathfrak{p}_{r_{p,q}} = |\Gamma_{p,q}|^2 \, \mathfrak{p}_{i_{p,q}}, \tag{28}$$

where for first-order ray tracing, the factor $|\Gamma_{p,q}|^2$ can be defined as the reflectance, whereas $\Gamma_{p,q}$ is the Fresnel reflection coefficient of the rough surface at the vertex $\mathbf{V}_{p,q}$ due to the incidence of the ray $\mathbf{i}_{p,q}$. It should be noted that, later on, the factor $\Gamma_{p,q}$ takes a more general definition for higher order ray tracing.

The incident electric field can be decomposed into horizontal and vertical components E_h^i and E_v^i, respectively, with respect to the rough surface at the point of incidence as follows.

$$\mathbf{E}^i = E_h^i \hat{a}_{hi_{p,q}} + E_v^i \hat{a}_{vi_{p,q}} \tag{29}$$

where $\hat{a}_{hi_{p,q}}$ and $\hat{a}_{vi_{p,q}}$ are the local vertical and horizontal polarization unit vectors, respectively, which can be calculated as follows.

$$\hat{a}_{hi_{p,q}} = \frac{\hat{a}_{n_{p,q}} \times \hat{a}_{k_i}}{\sin \vartheta_i}, \quad \hat{a}_{vi_{p,q}} = \hat{a}_{k_i} \times \hat{a}_{hi_{p,q}} \tag{30}$$

This requires the decomposition of the incident electric field $\mathbf{E}^i$ at each vertex of the rough surface into its components, that is

$$E_v^i = \mathbf{E}^i \cdot \hat{a}_{vi_{p,q}}, \quad E_h^i = \mathbf{E}^i \cdot \hat{a}_{hi_{p,q}} \tag{31}$$

If the incident electric field is confined to the plane of incidence (vertically polarized), which is the plane formed by $\hat{a}_{n_{p,q}}$ and $\hat{a}_{k_i}$, then the Fresnel reflection and transmission coefficients are given by the following expressions, respectively.

$$\Gamma = \Gamma_v = \frac{E_v^r}{E_v^i} = \frac{n_1 \cos \vartheta_t - n_2 \cos \vartheta_i}{n_1 \cos \vartheta_t + n_2 \cos \vartheta_i} \tag{32a}$$

$$T = T_v = \frac{E_v^t}{E_v^i} = \frac{2n_1 \cos \vartheta_i}{n_1 \cos \vartheta_t + n_2 \cos \vartheta_i} \tag{32b}$$

where n_1 and n_2 are the refractive indices of the media above and below the rough surface interface, respectively. If the incident electric field is normal to the plane of incidence (horizontally polarized), then the Fresnel reflection and transmission coefficients are given by the following expressions, respectively.

$$\Gamma = \Gamma_h = \frac{E_h^r}{E_h^i} = \frac{n_1 \cos \vartheta_i - n_2 \cos \vartheta_t}{n_1 \cos \vartheta_i + n_2 \cos \vartheta_t} \tag{33a}$$

$$T = T_h = \frac{E_h^t}{E_h^i} = \frac{2n_1 \cos \vartheta_i}{n_1 \cos \vartheta_i + n_2 \cos \vartheta_t} \tag{33b}$$

The local vertical and horizontal polarization unit vectors, respectively, for the reflected and transmitted rays can be calculated as follows.

$$\hat{a}_{hr_{p,q}} = \hat{a}_{hi_{p,q}}, \quad \hat{a}_{vr_{p,q}} = \hat{a}_{k_{r_{p,q}}} \times \hat{a}_{hr_{p,q}} \tag{34a}$$

$$\hat{a}_{ht_{p,q}} = \hat{a}_{hi_{p,q}}, \quad \hat{a}_{vt_{p,q}} = \hat{a}_{k_{t_{p,q}}} \times \hat{a}_{ht_{p,q}} \tag{34b}$$

The reflected and transmitted electric field vectors at the vertex $\mathbf{V}_{p,q}$ can be expressed as,

$$\mathbf{E}^r = E_h^r \hat{a}_{hr_{p,q}} + E_v^r \hat{a}_{vr_{p,q}} \tag{35a}$$

$$\mathbf{E}^t = E_h^t \hat{a}_{ht_{p,q}} + E_v^t \hat{a}_{vt_{p,q}} \tag{35b}$$

Usually, the incident electric field is composed of simultaneous vertically and horizontally polarized components. Substituting from Eqs. (32) and (33) into Eq. (35), one gets the following expressions for the reflected and transmitted field vectors.

$$\mathbf{E}^r = \Gamma_h E_h^i \hat{a}_{hr_{p,q}} + \Gamma_v E_v^i \hat{a}_{vr_{p,q}} \tag{36a}$$

$$\mathbf{E}^t = T_h E_h^i \hat{a}_{ht_{p,q}} + T_v E_v^i \hat{a}_{vt_{p,q}} \tag{36b}$$

In this case, the reflection coefficient at the vertex $\mathbf{V}_{p,q}$ can be calculated as follows.

$$E^r = E_h^r \cos \psi^r + E_v^r \sin \psi^r = \Gamma_h E_h^i \cos \psi^r + \Gamma_v E_v^i \sin \psi^r \tag{37}$$

where ψ^r is the angle subtended between the reflected electric field vector and $\hat{a}_h$ and can be expressed as,

$$\psi^r_{p,q} = \tan^{-1}\left(\frac{|E^r_v|}{|E^r_h|}\right) = \tan^{-1}\left(\frac{|\Gamma_v E^i_v|}{|\Gamma_h E^i_h|}\right) \tag{38a}$$

Also, let $\psi^i_{p,q}$ be the angle subtended between the incident electric field vector and $\hat{a}_{hi_{p,q}}$, and thereby, it can be expressed as,

$$\psi^i_{p,q} = \tan^{-1}\left(\frac{|E^i_v|}{|E^i_h|}\right) \tag{38b}$$

Thus, the Fresnel reflection coefficient can be expressed as,

$$\Gamma = \frac{E^r}{E^i} = \frac{\Gamma_h E^i_h \cos \psi^r_{p,q} + \Gamma_v E^i_v \sin \psi^r_{p,q}}{E^i_h \cos \psi^i_{p,q} + E^i_v \sin \psi^i_{p,q}} \tag{39}$$

3.2.8. Higher Order Scattering

A ray incident on a vertex $\mathbf{V}_{p,q}$ may be subjected to higher order reflection if the reflected ray collides with the rough surface at another vertex. Figure 4 shows the geometry required to discuss the condition that such a reflected ray should satisfy to collide with the rough surface. The angle between the ray reflected at the vertex $\mathbf{V}_{p,q}$ and the horizontal line, τ_r, can be expressed as

$$\tau_r = \frac{\pi}{2} - \cos^{-1} k_{r_z} \tag{40}$$

Figure 4. Condition required to consider higher order reflection of an incident ray.

According to the geometry presented in Figure 4, this ray will escape from other possible collisions with the rough surface if $\tau_r > \tau_D$, where τ_D is defined as,

$$\tau_D = \tan^{-1}\left(R_D - \frac{2z_{p,q}}{L_C}\right) \tag{41}$$

Thus, only the reflected ray that satisfies the following condition can probably collide with another point on the rough surface before going to the far zone causing second-order scattering.

$$\tau_r < \tau_D \tag{42}$$

For optimization of the computational complexity the reflected rays not satisfying the condition (42) will not be checked for higher order reflections on the rough surface.

It is clear from Eq. (42) that a higher surface roughness causes larger number of rays to be subjected to higher order reflections. Only for those reflected rays that satisfy Eq. (42) the following procedure is applied.

The ray that has the tth bounce at the vertex $\mathbf{V}_{p,q}$ collides with the rough surface at the vertex $\mathbf{V}_{u,v}$ if the following condition is satisfied

$$\hat{a}_{k_r}^{(t)} \cdot \hat{a}_{p,q}^{u,v} = 1, \tag{43}$$

where $\hat{a}_{k_r}^{(t)}$ is the unit vector in the direction of the reflected ray due to the tth bounce, and $\hat{a}_{p,q}^{u,v}$ is the unit vector in the direction from $\mathbf{V}_{p,q}$ to $\mathbf{V}_{u,v}$.

$$\hat{a}_{p,q}^{u,v} = \frac{\mathbf{V}_{u,v} - \mathbf{V}_{p,q}}{|\mathbf{V}_{u,v} - \mathbf{V}_{p,q}|} \tag{44}$$

If the condition (42) is satisfied, then this ray will have its $(t+1)$th bounce at the vertex $\mathbf{V}_{u,v}$ as shown in Figure 5. It should be noted that for each bounce of a ray the direction of the reflected ray is calculated as described in Section 3.2.3. The Fresnel coefficients at the points of reflection on the rough surface are calculated as described in 3.2.5. The phase associating a ray arriving at the far zone can be calculated as follows

$$\Delta\Phi_{p,q} = \frac{2\pi}{\lambda}\left(\Delta_{i_{p,q}} - \Delta_{r_{u,v}}\right) + \sum_{\nu=2}^{N_{O_{p,q}}} \frac{2\pi}{\lambda} D^{(\nu-1)} \tag{45}$$

where $D^{(\nu-1)}$ is the distance travelled by the reflected ray between the $(\nu-1)$th and the νth bounce points on the rough surface at the $(\nu-1)$th bounce point, where $\nu \geq 2$, $N_{O_{p,q}}$ is the maximum number of considered bounces, which is equal to the order of GTD-RT technique.
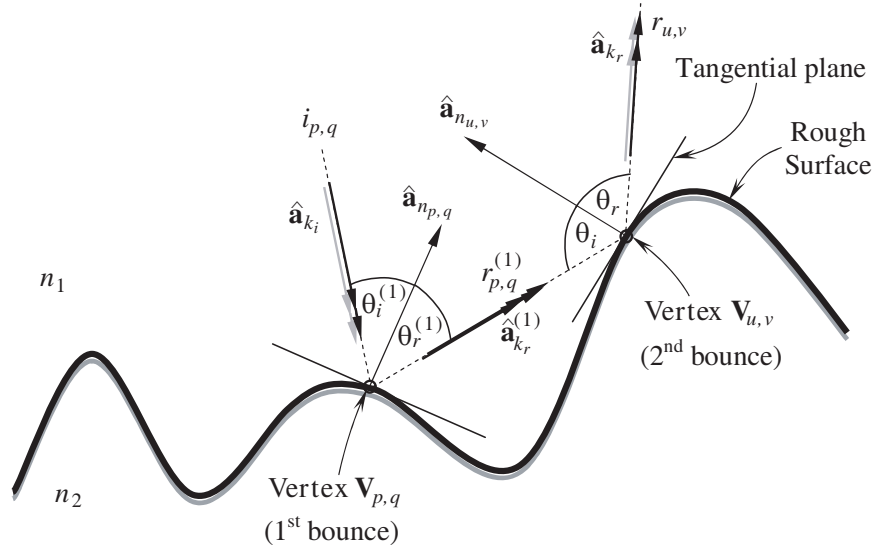
Figure 5. Double bounce of a ray at the vertices $\mathbf{V}_{p,q}$ and $\mathbf{V}_{u,v}$ on the rough surface.

3.3. Calculation of Scattering Pattern of the Optical Rays Incident on Rough Surfaces

Consider a large hemisphere of radius $R \to \infty$ covering the entire upper half-space ($z > 0$), as shown in Figure 6. Let the surface of the hemisphere be uniformly discretized in the θ- and ϕ-directions as shown in the figure. This results in $M \times N$ spherical surface segments whose areas can be evaluated as follows.

$$a_{mn} \approx R^2 \sin\theta_m \Delta\theta \Delta\phi, \quad m = 1, 2, \ldots, M, \quad n = 1, 2, \ldots, N \tag{46}$$

where,

$$\Delta\theta=\frac{\pi}{2M}, \quad \Delta\phi=\frac{2\pi}{N} \tag{47}$$

and,

$$\theta_m=\frac{2m-1}{2}\Delta\theta, \quad m=1,2,\ldots,M, \quad \phi_n=\frac{2n-1}{2}\Delta\phi, \quad n=1,2,\ldots,N \tag{48}$$

Substituting from (47) into (46), one gets,

$$a_{mn}\approx\frac{\pi^2}{MN}R^2\sin\theta_m, \quad m=1,2,\ldots,M, \quad n=1,2,\ldots,N \tag{49}$$
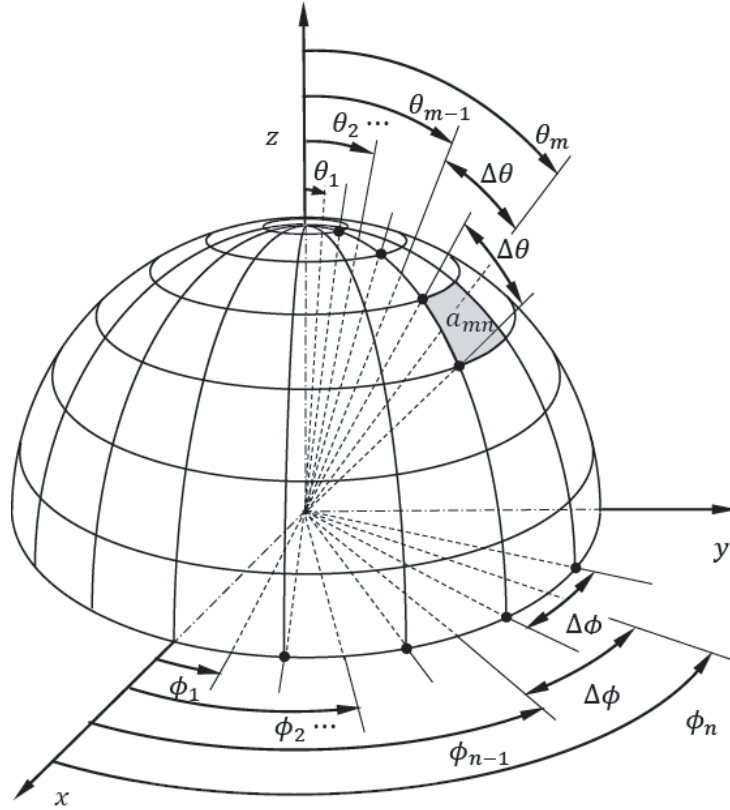
Figure 6. Segmented hemispherical surface above the rough surface with its (zero) mean height lying in the xy plane.

Consider a number of Q_i parallel rays incident in the direction $(\theta_i, \phi_i = 0)$ and uniformly distributed over the rough surface area under consideration as explained in Section 3. For accurate evaluation of the scattering pattern over the upper half space, we should have

$$Q_i\gg MN \tag{50}$$

Let the vertices, generated as described in Section 2 for the rough surface model, be interconnected using triangular patches. Each ray $i_{p,q}$ incident on a vertex $\mathbf{V}_{p,q}$ is reflected unless it is blocked from arriving at this vertex by some part of the rough surface. Hence the number of the reflected rays, Q_r is less than or equal to the number of the incident rays, Q_i.

$$Q_r\leq Q_i \tag{51}$$

However, the direction of the reflected ray obeys Snell's law and depends on the local vector representing the normal of the surface at this vertex (the normal of the rough surface at the point of incidence).

Define the two-angular direction, $\psi_{p,q}$ of the reflected ray $\mathfrak{r}_{p,q}$,

$$\psi_{p,q} \equiv (\theta_{p,q}, \phi_{p,q}) \tag{52}$$

where $\theta_{p,q}$ and $\phi_{p,q}$ are the angles between the reflected ray $\mathfrak{r}_{p,q}$ and the positive directions of the global z and x axes, respectively.

Define the two-angular zone $\Psi_{m,n}$,

$$\Psi_{m,n} \equiv \left\{ (\theta, \phi): \quad \theta_n - \frac{1}{2}\Delta\theta \leq \theta < \theta_n + \frac{1}{2}\Delta\phi, \quad \phi_n - \frac{1}{2}\Delta\phi \leq \phi < \phi_n + \frac{1}{2}\Delta\phi \right\} \tag{53}$$

The power density associated with the reflected ray $r_{p,q}$ can be expressed as follows

$$\frac{\mathfrak{p}_{r_{p,q}}}{a_{m,n}} = \frac{1}{2\eta_o} \left| E_{r_{p,q}} \right|^2 \tag{54}$$

where η_o is the intrinsic wave impedance of free space and $|E_{r_{p,q}}|$ is the magnitude of the electric field associated with the ray $r_{p,q}$. Making use of (28), one gets

$$\frac{|\Gamma_{p,q}|^2 \, p_{i_{p,q}}}{a_{m,n}} = \frac{1}{2\eta_o} \left| E_{r_{p,q}} \right|^2 \tag{55}$$

where,

$$\Gamma_{p,q} = \prod_{\nu=1}^{N_{O_{p,q}}} \Gamma^{(\nu)} \tag{56}$$

where $\Gamma^{(\nu)}$ is the Fresnel reflection coefficient of the ray $\mathfrak{i}_{p,q}$ (primarily incident on the vertex $\mathbf{V}_{p,q}$) at the bounce number ν, and $N_{O_{p,q}}$ is the total number of bounces to which the ray $\mathfrak{i}_{p,q}$ is subjected. It should be noted that $\Gamma^{(\nu)}$ is calculated using expressions (32), (33) or, generally, (39) by setting u and v to the values of the indices of the vertex at which the νth bounce occurs. Thus, the scattered electric field in the far zone can be evaluated as follows,

$$E_{mn} = E(\theta_m, \phi_n) = e^{-jk_oR} \sum_{\psi_{p,q} \in \Psi_{m,n}} \Upsilon_{p,q} \Gamma_{p,q} \sqrt{\frac{2\eta_o p_{i_{p,q}}}{a_{m,n}}} e^{-j\frac{2\pi}{\lambda}\Delta\Phi_{p,q}} \tag{57}$$

Making use of (48) and (56), the last expression can be written as,

$$E_{mn} = \frac{e^{-jk_oR}}{R} \frac{\sqrt{MN}}{\pi} \sqrt{\frac{\eta_o}{\sin\theta_m}} \sum_{\psi_{p,q} \in \Psi_{m,n}} \Upsilon_{p,q} \prod_{\nu=1}^{N_{O_{p,q}}} \Gamma^{(\nu)} \sqrt{\mathfrak{p}}_{i_{p,q}} e^{-j\frac{2\pi}{\lambda}\Delta\Phi_{p,q}} \tag{58}$$

4. RESULTS AND DISCUSSIONS

In this section, the accuracy of the results obtained by the GTD-RT method proposed for the assessment of optical scattering on rough surfaces is examined by comparison with the results obtained by experimental measurements. The improvement of the accuracy of the results obtained from higher-order GTD-RT is investigated by comparing the scattering patterns evaluated using a second-order to those obtained using the first-order GTD-RT. Also, the dependence of the optical scattering on the surface roughness and its dependence on the refractive index of the medium under the rough surface are studied. The effect of the resolution of the rough surface model on the accuracy of the evaluated scattering pattern is investigated. Finally, some of the numerical results obtained in the present work are compared to those of other published work.

4.1. Experimental Assessment of the Accuracy of the GTD-RT Method Proposed for Evaluating Scattering from Rough Surfaces

The GTD-RT method proposed in the present work for the evaluation of the far field pattern due to plane wave scattering on rough surfaces of arbitrary statistical parameters is assessed by comparison with some experimental measurements. The source of the incident plane wave is a light source of $\lambda = 635$ nm. The pattern of radiation from this source is presented in Figure 7 as measured by the optical power meter model Thorlabs®PM100 with the optical sensor S120B. The experimental setup for measuring the scattering pattern is presented in Figure 8. The rough sheet subjected to the incident beam is placed on a vertical wall. The light source is oriented so that the incident beam makes an angle of 45° with the normal to the sheet. The optical sensor connected to the power meter rotates from −90° to 90° with the normal to the sheet to read the intensity of the light scattered from the
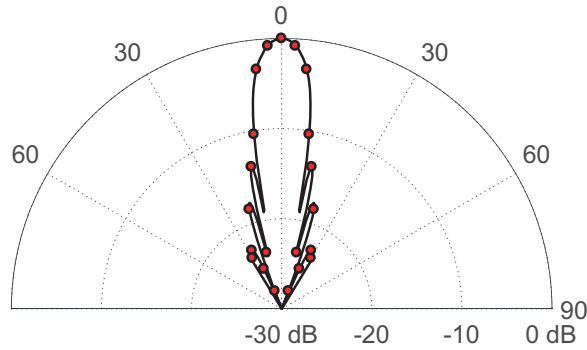
Figure 7. Radiation pattern of the light beam used for experimental measurements, $\lambda = 635$ nm.
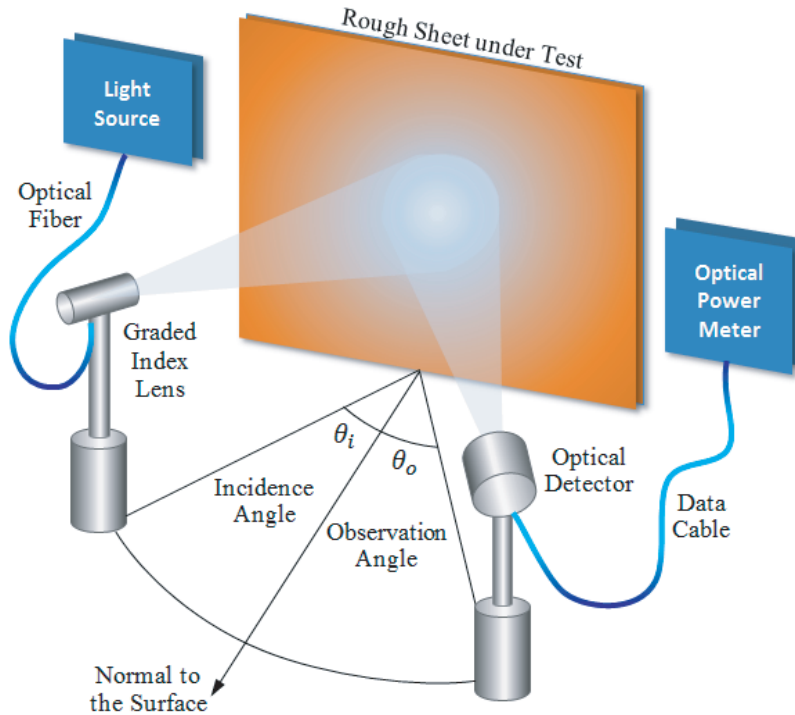
Figure 8. Experimental setup for measuring the scattering pattern due to a light beam incident on a sheet of rough surface using 635 nm laser source and Thorlabs®optical power meter model PM100 with optical detector model S120B.

flat sheet under test. Two white sheets of different roughness degrees are used for assessment of the proposed numerical technique: a glossy white sheet of roughness, $R_D = 0.09$, and a matte white sheet of roughness, $R_D = 0.225$.

A flat sheet of surface roughness $R_D = 0.09$, refractive index $n = 1.47$, is illuminated using the light beam shown in Figure 8. The optical scattering pattern is measured using the optical power meter through the experimental setup as described above. The measured scattering pattern is compared with that obtained using the second-order GTD-RT method proposed in the present work as shown in Figure 9(a). Due to the low degree of roughness of the reflecting surface the scattering pattern shows both specular and diffuse reflection properties. The agreement of the measured pattern with that numerically assessed shows the accuracy of the proposed GTD-RT method for evaluation of scattering of plane waves on rough surfaces. The same experiment is repeated for a flat sheet of surface roughness $R_D = 0.225$, refractive index $n = 1.51$. The measured scattering pattern is compared with that obtained using the second-order GTD-RT method proposed in the present work as shown in Figure 9(b). For the application of the GTD-RT, the correlation length of the rough surface model is assumed to be $L_C = 7.16\,\mu\text{m}$. Both the calculated and measured scattering patterns show diffuse reflection property of the reflecting surface due to the high degree of roughness. The measured scattering pattern agrees with that numerically assessed showing good accuracy of the proposed GTD-RT method.
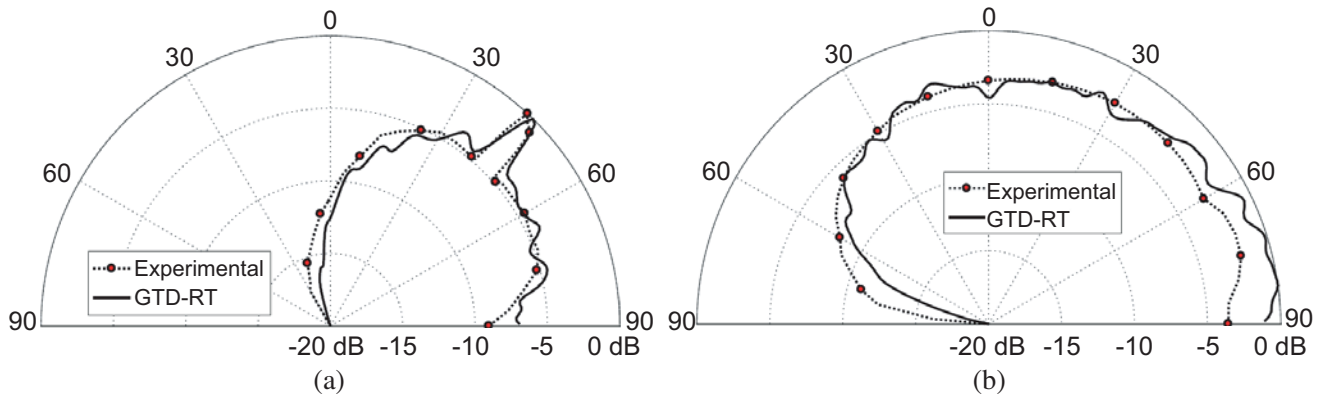
Figure 9. Comparison between the scattering patterns obtained through experimental measurements and GTD-RT method for V-polarized optical plane wave of $\lambda = 635\,\text{nm}$ incident on flat white sheets of different values of the roughness $L_C = 7.16\,\mu\text{m}$, $\theta_i^{(n)} = 45°$. (a) Glossy white sheet of $R_D = 0.09$, $n = 1.47$. (b) Matte white sheet of $R_D = 0.225$, $n = 1.51$.

It should be noted that the samples of the rough sheets selected for this experimental assessment of optical scattering have Gaussian height distribution and Gaussian correlation function with the indicated values of the correlation lengths, root-mean-squared heights, and refractive indices.

4.2. Comparison between the Accuracy of the First- and Second-Order GTD-RT Methods

The computational cost of applying second-order GTD-RT is considerably large compared to that of the first-order GTD-RD. The purpose of the present section is to compare the improvement of the solution obtained using the second-order GTD-RT over that obtained using the first-order method. For this purpose, three ensembles of rough surface models with different statistical parameters are generated. The ensemble has 20 different samples of rough surfaces generated with the same statistical parameters. The rough surface models of the first, second and third ensembles have roughness degrees $RD = 0.06, 0.10$, and 0.15, respectively where the correlation length is $L_C = 7.16\,\mu\text{m}$. For these three ensembles, Figures 10(a), (b), and (c) show the scattering patterns due to a plane wave incident at angle $45°$ normal to the surface. It is clear that in all the cases, the improvement due to the application of the 2nd order GTD-RT can be negligible even for high degrees of roughness. Considering that the results
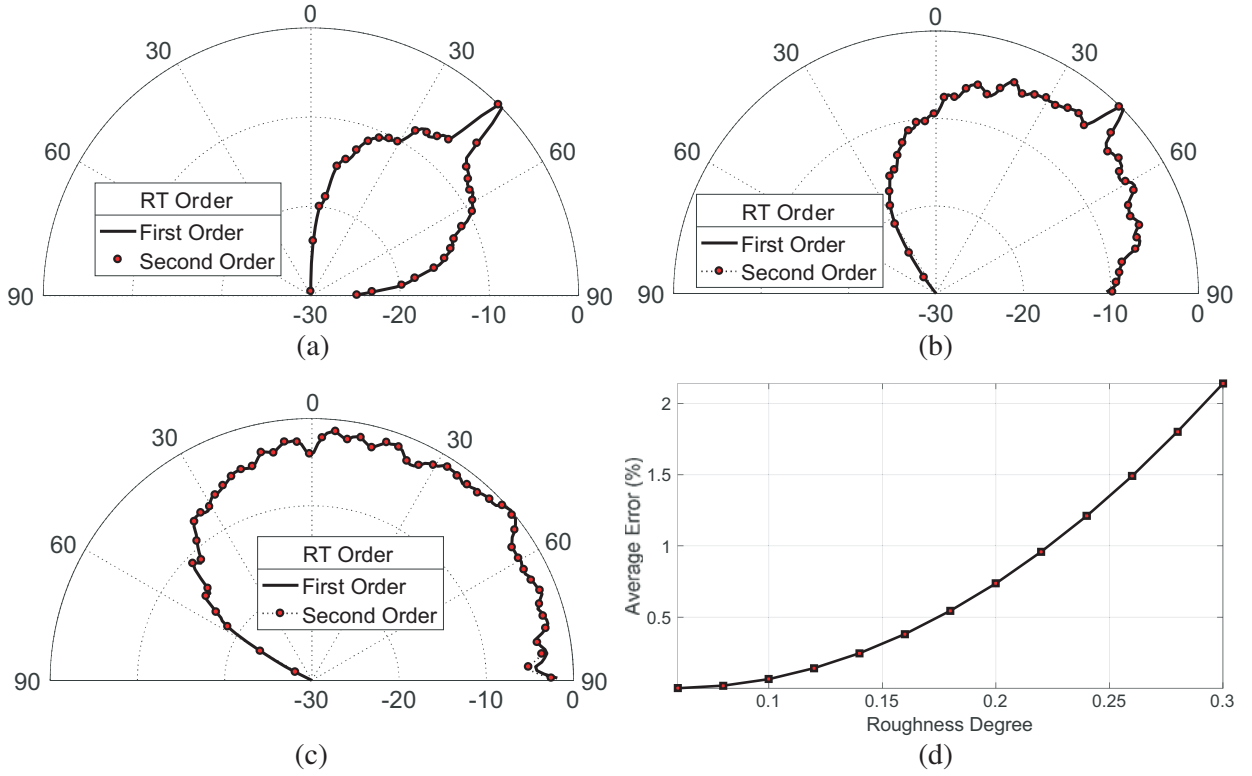
Figure 10. The scattering of V-polarized optical plane wave of $\lambda = 635\,\text{nm}$ incident on rough surfaces of $L_C = 7.16\,\mu\text{m}$, $\theta_i^{(n)} = 45°$, $n = 3.16$ resolution 2000×2000 vertices, evaluated by the application of first-order and second-order GTD-RT. (a) Scattering patterns, $R_D = 0.06$. (b) Scattering patterns, $R_D = 0.1$. (c) Scattering patterns, $R_D = 0.15$. (d) Average error against the degree of roughness.

obtained by the 2nd order method are more accurate than those obtained by the 1st order method, the average error in the scattering coefficients obtained by the first-order ray tracing can be defined as: the difference between the average of the scattering coefficients obtained by the first-order ray tracing over all the directions of the half space and that average obtained by the second-order ray tracing. The average percent error is defined as the ratio between this difference and the averaged scattering coefficients obtained by the second-order ray tracing. This error can be calculated as follows.

$$\text{Average error }(\%) = \sum_{\theta,\phi} \frac{\left| E_{1st}^r\left(\theta,\phi\right) - E_{2nd}^r\left(\theta,\phi\right)\right|}{\left| E_{2nd}^r\left(\theta,\phi\right)\right|} \times 100\% \tag{59}$$

where, $E_{1st}^r(\theta,\phi)$ and $E_{2nd}^r(\theta,\phi)$ are the scattered electric fields in the direction (θ,ϕ) calculated using the 1st and 2nd order RT, respectively.

Figure 10(d) shows the dependence of such average percent error on the surface roughness. It is clear that the error due to the application of the 1st order method instead of the 2nd order method increases with increasing the surface roughness. However, even for highly rough surfaces ($RD = 0.3$), the percentage error does not exceed 2.5%. As the application of the 2nd or higher order GTD-RT is computationally complex, the negligible improvement of the accuracy over the 1st order GTD-RT makes the latter be more efficient for evaluating optical scattering from rough surfaces.

4.3. Reflection and Transmission through Rough Surfaces

The method developed in the present works accounts for the calculation of the electromagnetic power reflected to the upper half-space as well as the power transmitted to the lower half-space. Figure 11 shows the scattering pattern (both reflection and transmission) due to a plane wave incident on horizontal

rough surfaces of relatively low degree of roughness ($R_D = 0.08, 0.10$). The plane wave is incident at an angle of $45°$ with the vertical direction as indicated by the arrow labeled i. As determined by Snell's law, the direction of specular reflection is indicated in the figure by the arrow labeled r and the direction of specular refraction (transmission) is indicated by the arrow labeled t. It is shown that, due to the relatively low roughness of the surface, both the reflection and transmission are mainly specular with a low level of diffuse scattering. Also, it is shown that as the refractive index increases the reflected power increases on the account of the transmitted power. For low values of the refractive index $n = 1.5$, the transmitted power is considerably larger than the reflected power as shown in Figure 11(a). For high
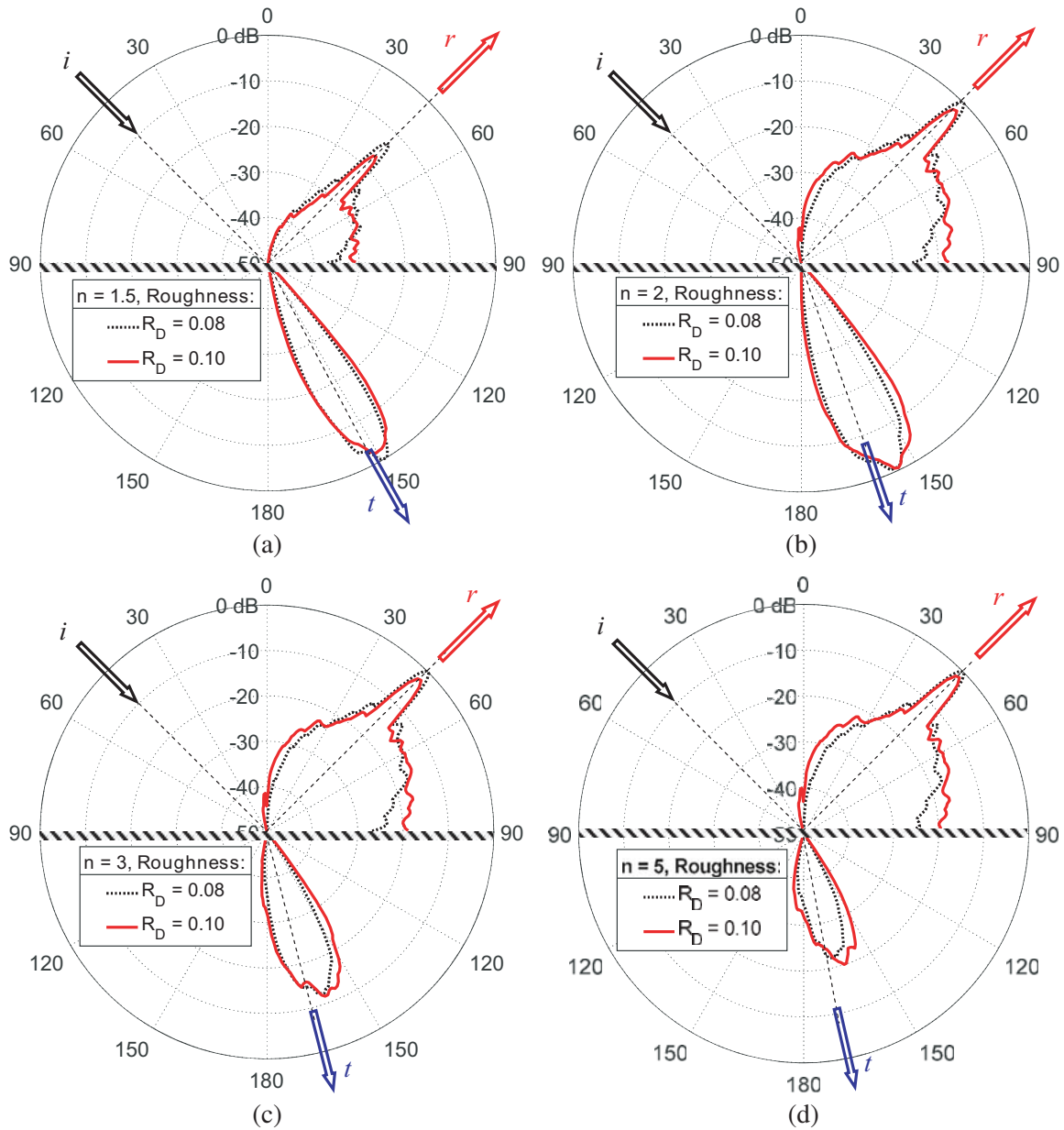
Figure 11. The patterns of scattering (reflection and transmission) of a plane wave of $\lambda = 1000\,\text{nm}$ incident on ($20\,\mu\text{m} \times 20\,\mu\text{m}$) rough surfaces of $L_C = 2\,\mu\text{m}$ resolution 1000×1000 vertices, and different values of the refractive index, $\theta_i^{(n)} = 45°$. The direction of specular refraction (transmission) according to Snell's law is given by the value θ_t indicated for each case. (a) $\theta_t = 28.1°$. (b) $\theta_t = 20.7°$. (c) $\theta_t = 13.6°$. (d) $\theta_t = 8.1°$.

values of the refractive index $n = 5$, the reflected power is considerably larger than the transmitted power as shown in Figure 11(d).

4.4. Dependence of the Scattering Pattern on the Surface Roughness

As experimentally demonstrated, in Section 4.1 the electromagnetic scattering from a surface of medium roughness exhibits both specular and diffuse properties whereas a highly rough surface causes only diffuse scattering. The scattering pattern for a rough surface is strongly dependent on the surface roughness as shown in Figure 12 for different values of the angle of incidence. It is clear that the beam width of the scattered optical power increases with increasing the roughness degree. For low roughness $(RD = 0.01)$, the scattering pattern has a high narrow peak in the specular direction determined by Snell's law and insignificant diffuse scattering over the upper space. With increasing the surface roughness $(RD = 0.05, 0.1)$ the diffuse scattering increases whereas the specular scattering decreases and, hence, the scattered beam is broadened and the peak in the specular direction is weakened. For high degrees of roughness, $(RD = 0.15)$, the rough surface produces nearly complete diffuse scattering where the peak due to specular scattering is almost diminished. Also, it is clear that the angle of incidence affects the shape and width of the scattering pattern, where the specular component of the scattered beam seems to be greater with increasing the angle of incidence for a given value of the surface roughness. In the meantime, the backscatter decreases with increasing the angle of incidence for a given value of the surface roughness. Generally, with increasing the surface roughness, irrespective of the angle of incidence $\theta_i^{(n)}$, the backscattered field is clearly increased.
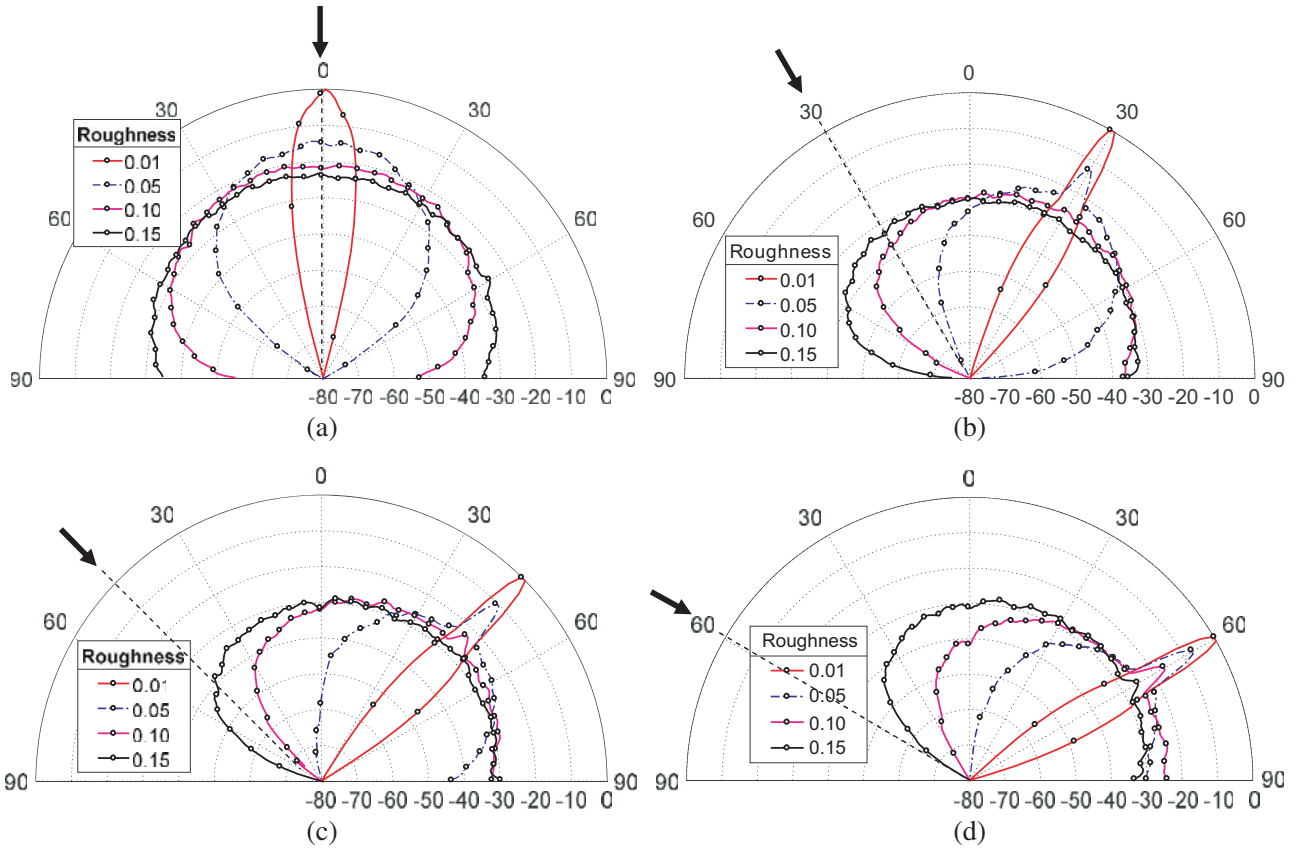
Figure 12. The scattering patterns due to V-polarized plane wave incident on a rough surface model of resolution 1000×1000 vertices, $n = 3.16$, $L_C = 7.16\,\mu\text{m}$ with different values of the degree of roughness and the angle of incidence. (a) $\theta_i^{(n)} = 0°$. (b) $\theta_i^{(n)} = 30°$. (c) $\theta_i^{(n)} = 45°$. (d) $\theta_i^{(n)} = 60°$.

4.5. Dependence of the Accuracy of the Calculated Scattering Pattern on the Resolution of the Rough Surface Model

To get accurate results for the scattering coefficients in the far zone due to a plane wave incident on a rough surface using GTD-RT, the number of the incident rays should be large enough, as given by Eq. (50), to get accurate ray representation of the scattered power distribution over the half-space. The larger the number of incident rays the more accurate the obtained scattering coefficients. As the number of the incident rays is equal to the number of vertices on the rough surface, high resolution of the rough surface is required to get accurate results for the scattering coefficients in the different directions. The case of a surface of roughness $R_D = 0.1$ combines the properties of both diffuse and specular reflections. For this reason, such a roughness is considered to examine the effect of the rough surface resolution on the accuracy of the results obtained for the scattering pattern.

Figure 13 shows the scattering patterns obtained due to a vertically polarized plane incident on a rough surface model with different resolutions (number of vertices constructing its geometric model). For low resolution model (250×250), the scattering pattern seems to have large errors especially in the direction normal to the rough surface and in the specular direction. With increasing the resolution, the accuracy is improved asymptotically (especially in the specular direction) to get accurate results for a rough surface model of resolution (3000×3000).
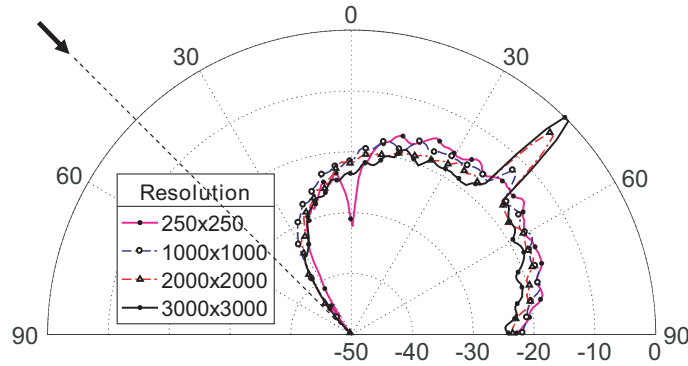
Figure 13. The scattering patterns due to V-polarized plane wave incident in the direction $\theta_i^{(n)} = 45°$ on a $63.5 \times 63.5 \, \mu m$ rough surface model of different resolutions; $R_D = 0.1$; $\lambda = 635 \, nm$, $L_C = 7.16 \, \mu m$.

Very accurate results for the scattering coefficients over the upper half-space are obtained for a rough surface model of resolution (3000×3000). Increasing the resolution beyond this value does not have a significant improvement of the obtained accuracy. Thereby, the relative error of the scattering coefficients due to limited surface resolution can be defined as: the difference between the average of the scattering coefficients obtained using a specific geometric resolution over all the directions of the half space and that average obtained using geometric resolution of (3000×3000). The relative error is defined as the ratio between this difference and the averaged scattering coefficients obtained using a resolution of (3000×3000). This error can be calculated as follows.

$$\text{Relative error} = \sum_{\theta, \phi} \frac{\left| E_Q^r(\theta, \phi) - E_{3k}^r(\theta, \phi) \right|}{\left| E_{3k}^r(\theta, \phi) \right|} \tag{60}$$

where $E_Q^r(\theta, \phi)$ and $E_{3k}^r(\theta, \phi)$ are the scattered electric fields in the direction (θ, ϕ) for rough surface resolutions $Q \times Q$ and 3000×3000, respectively, where $Q < 3000$.

The dependence of this error due to the limited resolution of the rough surface for different values of the surface roughness and angle of incidence is presented in Figure 14. It is clear that the relative error, averaged over all the directions in the upper space, is decreased with increasing the resolution of the rough surface model. Also, for a given resolution, the error increases with decreasing the surface roughness as shown in Figure 14(a) and, also, increases with increasing the angle of incidence as shown in Figure 14(b).

(a)   (b)
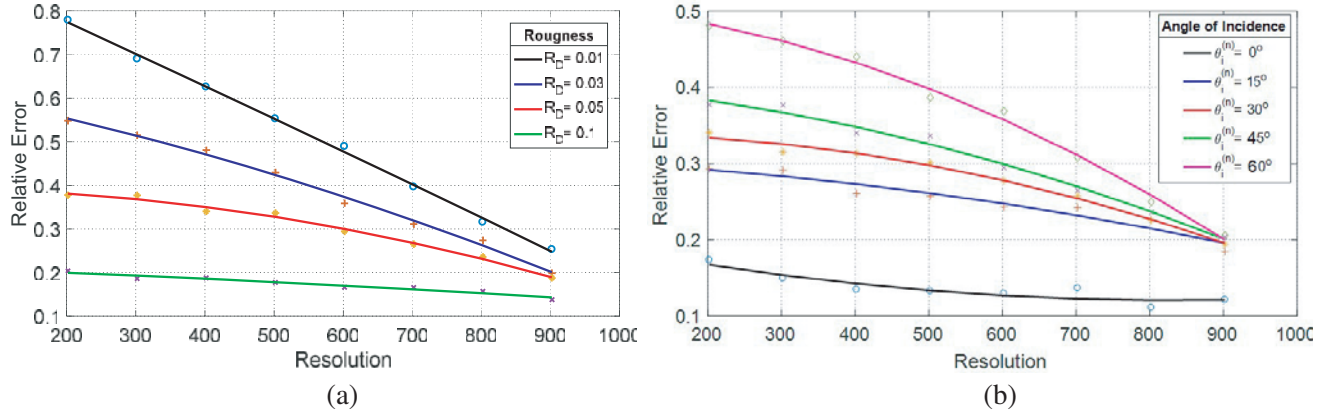
Figure 14. Dependence of the relative error of the calculated scattering pattern due to V-polarized plane wave incident on a rough surface on the resolution of the geometric model of the rough surface for different values of the surface roughness and angle of incidence. (a) $\theta_i^{(n)} = 45°$. (b) $R_D = 0.05$.

4.6. Dependence of the Scattering on the Polarization of Incident Field

The scattering of either H-polarized or V-polarized plane wave incident on a rough surface which is an interface between the free space and a dielectric medium is investigated for different values of the surface roughness and refractive indices. As shown in Figure 15(a), for high value of the refractive index ($n = 10$), the scattering patterns for the H-polarized and the V-polarized waves are very close to each other. As shown in Figures 15(b), 16(a), 16(b) for lower values of the refractive index ($n = 3.16$, $n = 1.5$), respectively, the scattering patterns for the two polarizations are different from each other. It is clear that decreasing the refractive index has the effect of increasing the *backscattering* of the V-polarized wave and increasing the scattering of the H-polarized wave in the *forward* direction parallel to the surface. On the other side, increasing the roughness of the surface has the effect of decreasing the specular scattering on behalf of the diffuse scattering for both types of polarization, which is shown by comparison between the scattering patterns presented in Figures 16(a) and 16(b).

(a)   (b)
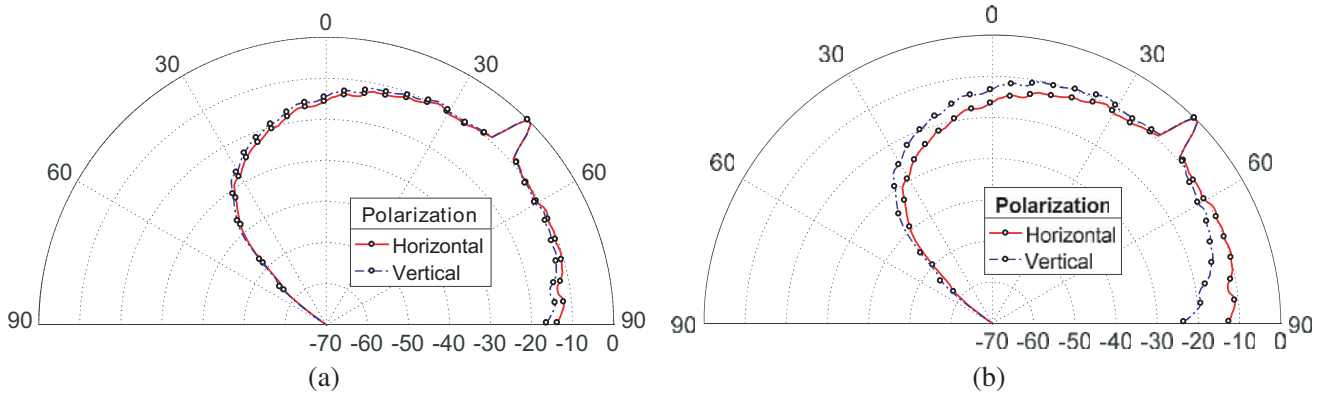
Figure 15. The scattering patterns due to H-polarized and V-polarized plane waves incident in the direction $\theta_i^{(n)} = 45°$ on a $63.5 \times 63.5 \, \mu\text{m}$ rough surface of resolution 1500×1500 vertices and $R_D = 0.10$; $\lambda = 635 \, \text{nm}$, $L_C = 7.16 \, \mu\text{m}$. (a) $n = 10$. (b) $n = 3.16$.

4.7. Comparison with Other Methods Based on the GO and KA

The scattering coefficients are calculated for a rough surface using the GO approximation and compared with rigorous electromagnetic solution based on the extinction theorem in [28]. For a perfectly
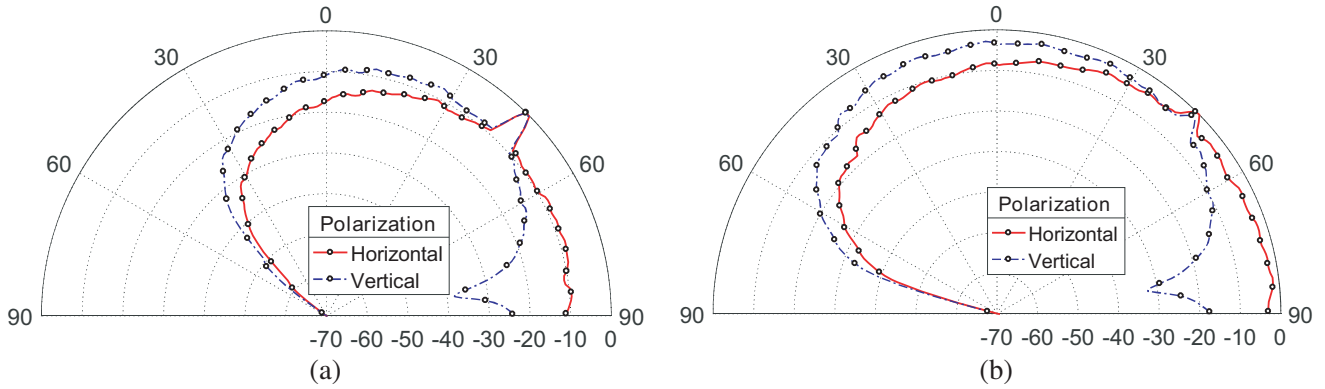
Figure 16. The scattering patterns due to H-polarized and V-polarized plane waves incident in the direction $\theta_i^{(n)} = 45°$ on a $63.5 \times 63.5\,\mu\text{m}$ rough surface of resolution 1500×1500 vertices; $\lambda = 635\,\text{nm}$, $L_C = 7.16\,\mu\text{m}$, $n = 1.5$. (a) $R_D = 0.10$. (b) $R_D = 0.15$.

conducting rough surface model of $R_D = 0.2$ and $L_c = 2\lambda$ the optical scattering pattern is obtained using the GO as described in [28] and compared with the exact solution as shown in Figure 17(a). The GTD-RT method proposed in the present work is applied to an ensemble of 10 samples of rough surface models of the same statistical properties where the ensemble average of the obtained scattering patterns is compared to both the exact solution and that of [28]. It is shown that the scattering pattern obtained using the GTD-RT algorithm proposed in the present work is closer to the exact solution than that obtained in [28] using the GO.

For a very rough perfectly conducting surface of roughness $R_D = 1.1$ and correlation length $L_c = 1.8\lambda$, the scattering pattern obtained using the GTD-RT algorithm proposed in the present work (averaged over an ensemble of size 10) is compared to that obtained in [30] using the modified second-order Kirchhoff approximation as well as the exact solution obtained by Monte Carlo averaging of the MoM solution of the integral equation. As shown in Figure 17(b), the solution obtained by the proposed GTD-RT algorithm of the present work is closer to the exact solution than that obtained using the Kirchhoff approximation.

For a two-dimensional perfectly conducting surface model of roughness $R_D = 0.38$ and correlation length $L_c = 2.3\lambda$, the scattering pattern obtained using the GTD-RT proposed in the present work (averaged over an ensemble of size 10) is compared to that obtained in [29] using the GO showing good agreement as shown in Figure 17(c).

At the end of presenting the numerical results of the present work, it may be useful to highlight the contributions of the present work in the context of the past methods proposed for the same purpose. The advantages of the proposed GTD-RT method are briefly discussed versus the most commonly used methods: Monte Carlo averaging, KA, and GO. Monte Carlo calculations are used for ensemble averaging the MoM solution of the exact integral equation formulated for the scattered field on a rough surface. Hence, the Monte Carlo solution is, definitely, more accurate than those obtained by the GO and the KA. The main computational drawback of the Monte Carlo method is that it leads to a certain amount of deviation from the correct average that decreases with increasing the number of generated samples of the rough surface models [33]. Thus, the Monte Carlo method requires a large ensemble of the surface models to calculate an accurate average value of the scattered field. As the Monte Carlo method can be considered an exact solution of the integral equation for the scattered field, its solution is usually taken as the reference to which the results obtained using the GO and KA are compared for verification of accuracy [28, 30]. The Monte Carlo solution requires a large number of the rough model samples (ensemble size is usually ranges a few hundreds to one thousand). In the present work, the ensemble averaging is, also, required for the proposed GTD-RT algorithm for the assessment of scattering from rough surfaces. However, it is found, by numerical experimentation, that an ensemble size that ranges from only 5 to 10 can be enough to get more accurate results than those available in the published work (Section 4.7 show three examples of comparison). Although the GTD-RT algorithm
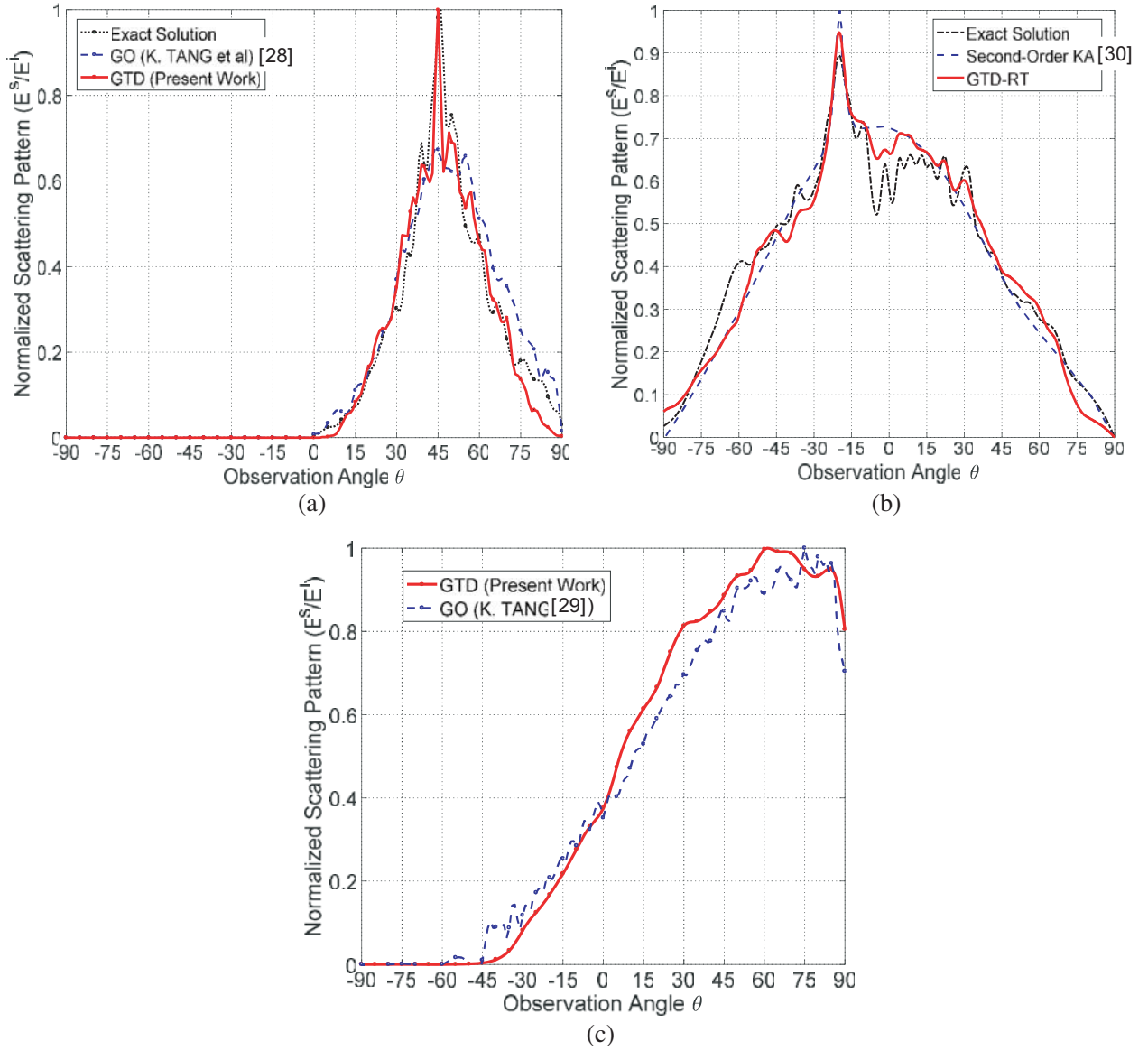
Figure 17. The scattering patterns due to a plane wave incident in the direction $\theta_i^{(n)} = 45°$ on a perfectly conducting rough surface of dimensions $100\lambda \times 100\lambda$ and resolution 1000×1 vertices compared to other published results. (a) $R_D = 0.2$, $L_c = 2\lambda$, $\theta_i^{(n)} = 45°$. (b) $R_D = 1.1$, $L_c = 1.8\lambda$, $\theta_i^{(n)} = 20°$. (c) $R_D = 0.38$, $L_c = 2.3\lambda$, $\theta_i^{(n)} = 45°$.

proposed in the present study requires ensemble averaging, the overall computational efficiency of the proposed method is better than those of the Monte Carlo, KA and GO methods owing to the very small ensemble size and due to the efficiency of method proposed for the distribution of the points of the rough surface that are selected to receive the incident rays.

Most of the past published papers implementing Monte Carlo simulation usually use an exact technique like the method of moments (MoM), finite element (FE), and finite-difference-time-domain (FDTD) methods or another rigorous numerical technique to get accurate field calculations [34]. The major achievement of the method proposed in the present paper is the accuracy of the obtained scattered field together with the computational efficiency of the applied algorithm. As shown from the comparisons presented in Figure 17, the solution obtained by the proposed GTD-RT algorithm may be closer to the exact solution than those of the GO and KA methods. This considered as improvement of the accuracy.
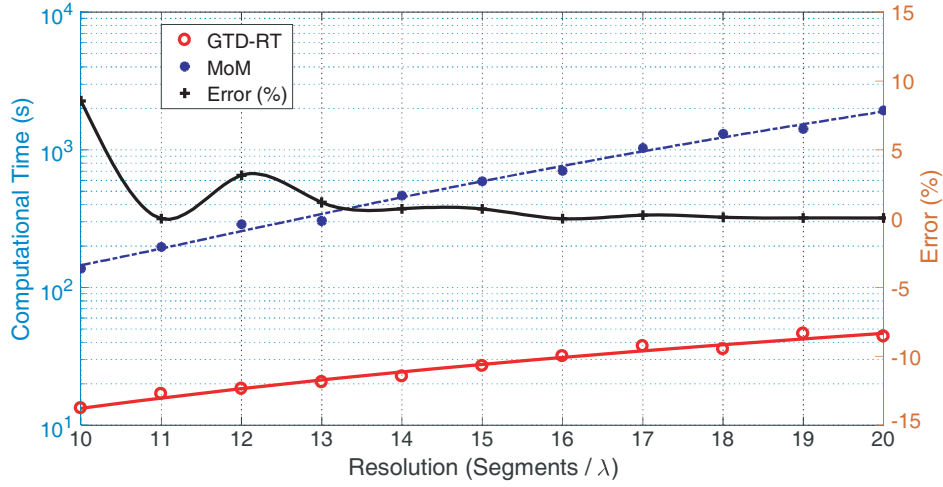
Figure 18. The computational time taken by the GTD-RT method compared to that taken by the MoM to calculate the scattering patterns (together with corresponding error) due to a plane wave incident in the direction $\theta_i^{(n)} = 45°$ on a perfectly conducting rough surface of dimensions $10\lambda \times 10\lambda$ with increasing the resolution; $R_D = 0.38$, $L_c = 2.3\lambda$, $\theta_i^{(n)} = 45°$.

On the other hand, the proposed algorithm is shown to be computationally efficient as it uses a very small-size ensemble of the rough surface realizations (5–20 may be acceptable) when compared with the "exact" Monte Carlo method. For assessment of the computational time improvement achieved by the proposed GTD-RT method, the MoM, as described in [35], is applied to evaluate the pattern of the scattered field due to a plane wave incident on a given realization of a perfectly conducting rough surface. As shown in Figure 18, the computational time taken by the proposed GTD-RT method for calculating the scattered field on the same rough surface realization is considerably lower than that taken by the MoM.

Considering that the scattered field obtained using the MoM is more accurate than that obtained by the GTD-RT method, the error in the scattering coefficients obtained by the GTD-RT method can be defined as the difference between the average of the scattering coefficients obtained by the GTD-RT over all the directions of the half space and that average obtained by the MoM. The percent error is defined as the ratio between this difference and the averaged scattering coefficients obtained by the MoM. This error can be calculated as follows.

$$\text{Error}\,(\%) = \sum_{\theta,\phi} \frac{\left|E_{GTD}^r\,(\theta,\phi) - E_{MoM}^r\,(\theta,\phi)\right|}{\left|E_{MoM}^r\,(\theta,\phi)\right|} \times 100\% \tag{61}$$

where, $E_{GTD}^r(\theta,\phi)$ and $E_{MoM}^r(\theta,\phi)$ are the scattered electric fields in the direction (θ,ϕ) calculated using the GTD-RT and the MoM, respectively. It is shown that, with increasing the resolution (λ/Δ) of the rough surface model, the resulting error in the scattered field calculated by the GTD-RT is reduced and almost vanishes for high resolution.

5. CONCLUSION

The GTD-RT technique is proposed to evaluate the electromagnetic scattering from a rough surface of quite arbitrary statistical parameters. The method of generating the geometrical model of the rough surface is explained. The Fresnel reflection model is applied for arbitrary electrical and optical properties of the rough surface material taking into account the polarization of the incident plane wave to obtain the scattering patterns for both the power reflected to the upper half-space and the power transmitted into the medium covered by the rough surface. The algorithm developed in the present work can be considered a higher order GTD-RT that accounts for multiple bounces of an incident ray. The accuracy

of the obtained results is verified through the comparison with the experimental measurements of the scattering pattern of a light beam incident on samples of rough sheets with specific statistical properties. Some of the obtained results are compared to other published results using both the GO approximation and the second-order Kirchhoff's approximation showing good agreement. The presented numerical results are concerned with studying the dependence of the resulting scattering pattern on the surface roughness, refractive index, angle of incidence, and the resolution of the geometric model of the rough surface. Also, it is shown that, for limited resolution of the rough surface model, the accuracy of the calculated scattered field depends on the angle of incidence of the primary beam and the surface roughness. The proposed GTD-RT method can be considered more accurate than the GO approximation and KA methods and more computationally efficient than Monte Carlo averaging method.

REFERENCES

1. Manallah, A. and M. Bouafia, "Application of the technique of total integrated scattering of light for micro-roughness evaluation of polished surfaces," *Physics Procedia*, Vol. 21, 174–179, 2011.

2. Germer, T. A., "Polarized light diffusely scattered under smooth and rough interfaces," *Polarization Science and Remote Sensing*, Vol. 5158, 193–205, International Society for Optics and Photonics, December 2003.

3. Pinel, N., C. Bourlier, and J. Saillard, "Degree of roughness of rough layers: Extensions of the Rayleigh roughness criterion and some applications," *Progress In Electromagnetics Research B*, Vol. 19, 41–63, 2010.

4. Ruiz-Cortés, V. A. and J. C. Dainty, "Experimental light-scattering measurements from large-scale composite randomly rough surfaces," *JOSA A*, Vol. 19, No. 10, 2043–2052, 2002.

5. Manallah, A. and M. Bouafia, "Application of the technique of total integrated scattering of light for micro-roughness evaluation of polished surfaces," *Physics Procedia*, Vol. 21, 174–179, 2011.

6. Spencer, M. F. and M. W. Hyde, IV, "Rough surface scattering for active-illumination systems," *SPIE Newsroom*, 1–2, 2013.

7. Jafari, G. R., S. M. Mahdavi, A. Iraji Zad, and P. Kaghazchi, "Characterization of etched glass surfaces by wave scattering," *Surface and Interface Analysis: An International Journal Devoted to the Development and Application of Techniques for the Analysis of Surfaces, Interfaces and Thin Films*, Vol. 37 No. 7, 641–645, 2005.

8. Zamani, M., F. Shafiei, S. M. Fazeli, M. C. Downer, and G. R. Jafari, "Analytic height correlation function of rough surfaces derived from light scattering," *Physical Review E*, Vol. 94, No. 4, 042809, 2016.

9. Sanamzadeh, M., L. Tsang, J. T. Johnson, R. J. Burkholder, and S. Tan, "Scattering of electromagnetic waves from 3D multilayer random rough surfaces based on the second-order small perturbation method: Energy conservation, reflectivity, and emissivity," *Journal of the Optical Society of America A*, Vol. 34, No. 3, 395–409, 2017.

10. Wu, Z. S., J. J. Zhang, and L. Zhao, "Composite electromagnetic scattering from the plate target above a one-dimensional sea surface: Taking the diffraction into account," *Progress In Electromagnetics Research*, Vol. 92, 317–331, 2009.

11. Guo, L. and Z. Wu, "Application of the extended boundary condition method to electromagnetic scattering from rough dielectric fractal sea surface," *Journal of Electromagnetic Waves and Applications*, Vol. 18, No. 9, 1219–1234, 2004.

12. Qamar, H. H., K. F. A. Hussein, and M. B. El-Mashade, "Assessment of signal strength in indoor optical wireless communications using diffuse infrared radiation," *2019 36th National Radio Science Conference (NRSC)*, IEEE, 2019.

13. Harvey, J. E., J. J. Goshy, and R. N. Pfisterer, "Modeling stray light from rough surfaces and subsurface scatter," *Reflection, Scattering, and Diffraction from Surfaces IV*, Vol. 9205, 92050I, International Society for Optics and Photonics, September 2014.

14. Beckmann, P., "Scattering by composite rough surfaces," *Proceedings of the IEEE*, Vol. 53, No. 8, 1012–1015, 1965.

15. Hyde, M. W., S. Basu, M. F. Spencer, S. J. Cusumano, and S. T. Fiorino, "Physical optics solution for the scattering of a partially-coherent wave from a statistically rough material surface," *Optics Express*, Vol. 21, No. 6, 6807–6825, 2013.

16. Elfouhaily, T. M. and C. A. Guérin, "A critical survey of approximate scattering wave theories from random rough surfaces," *Waves in Random Media*, Vol. 14, No. 4, R1–R40, 2004.

17. Rice, S., "Reflection of electromagnetic waves from slightly rough surfaces," *Communications on Pure and Applied Mathematics*, Vol. 4, No. 2–3, 351–378, 1951.

18. Tian, J., J. Tong, J. Shi, and L. Gui, "A new approximate fast method of computing the scattering from multilayer rough surfaces based on the Kirchhoff approximation," *Radio Science*, Vol. 52, No. 2, 186–193, 2017.

19. Thorsos, E. I., "The validity of the Kirchhoff approximation for rough surface scattering using a Gaussian roughness spectrum," *Journal of the Acoustical Society of America*, Vol. 83, No. 1, 78–92, 1988.

20. Demir, M. A. and J. T. Johnson, "Fourth-and higher-order small-perturbation solution for scattering from dielectric rough surfaces," *Journal of the Optical Society of America A*, Vol. 20, No. 12, 2330–2337, 2003.

21. Voti, R., G. Leahu, S. Gaetani, C. Sibilia, V. Violante, E. Castagna, and M. Bertolotti, "Light scattering from a rough metal surface: Theory and experiment," *Journal of the Optical Society of America B*, Vol. 26, No. 8, 1585–1593, 2009.

22. Vorburger, T., R. Silver, R. Brodmann, B. Brodmann, and J. Seewig, "Light scattering methods," *Optical Measurements of Surface Topography*, 287–311, R. Leach (Ed.), Springer, Berlin, 2011.

23. Sanchez-Gil, J. A. and M. Nieto-Vesperinas, "Light scattering from random rough dielectric surfaces," *Journal of the Optical Society of America A*, Vol. 8, No. 8, 1270–1286, 1991.

24. Nordam, T., P. Letnes, and I. Simonsen, "Numerical simulations of scattering of light from two-dimensional rough surfaces using the reduced Rayleigh equation," *Frontiers in Physics*, Vol. 1, 8, 2013.

25. Ishimaru, A. and J. Chen, "Scattering from very rough metallic and dielectric surfaces: A theory based on the modified Kirchhoff approximation," *Waves in Random Media*, Vol. 1, No. 1, 21–34, 1991.

26. Bruce, N. and J. Dainty, "Multiple scattering from rough dielectric and metal surfaces using the Kirchhoff approximation," *Journal of Modern Optics*, Vol. 38, No. 8, 1471–1481, 1991.

27. Bruce, N., "Multiple scatter of vector electromagnetic waves from rough metal surfaces with infinite slopes using the Kirchhoff approximation," *Waves in Random and Complex Media*, Vol. 21, No. 2, 362–377, 2011.

28. Tang, K., R. Dimenna, and R. Buckius, "Regions of validity of the geometric optics approximation for angular scattering from very rough surfaces," *International Journal of Heat and Mass Transfer*, Vol. 40, No. 1, 49–59, 1996.

29. Tang, K. and R. Buckius, "The geometric optics approximation for reflection from two-dimensional random rough surfaces," *International Journal of Heat and Mass Transfer*, Vol. 41, No. 13, 2037–2047, 1998.

30. Ishimaru, A. and J. Chen, "Scattering from very rough surfaces based on the modified second-order Kirchhoff approximation with angular and propagation shadowing," *The Journal of the Acoustical Society of America*, Vol. 88, No. 4, 1877–1883, 1990.

31. Holliday, D., "Resolution of a controversy surrounding the Kirchhoff approach and the small perturbation method in rough surface scattering theory," *IEEE Transactions on Antennas and Propagation*, Vol. 35, No. 1, 120–122, 1987.

32. Soliman, S. A. M., A. E. Farahat, K. F. A. Hussein, and A. A. Ammar, "Spatial domain generation of random surface using Savitzky-Golay filter for simulation of electromagnetic polarimetric systems," *Applied Computational Electromagnetics Society Journal*, Vol. 34, No. 1, 2019.

33. Millet, F. and K. Warnick, "Validity of rough surface backscattering models," *Waves in Random Media*, Vol. 14, No. 3, 327–347, 2004.

34. Shi, F., W. Choi, M. J. S. Lowe, E. A. Skelton, and R. V. Craster, "The validity of Kirchhoff theory for scattering of elastic waves from rough surfaces," *Proceedings of the Royal Society A: Mathematical, Physical and Engineering Sciences*, Vol. 471, No. 2178, 20140977, 2015.

35. Hussein, K. F. A., "Fast computational algorithm for EFIE applied to arbitrarily-shaped conducting surfaces," *Progress In Electromagnetics Research*, Vol. 68, 339–357, 2007.